Arabian Journal for Science and Engineering
https://doi.org/10.1007/s13369-022-06601-2

RESEARCH ARTICLE-CIVIL ENGINEERING

Carbon Fiber-Reinforced Polymer Rod Embedment Depth Influence on Concrete Strengthening

Ay Lie Han[1] · Hsuan-Teh Hu[2,3] · Buntara S. Gan[4] · Fu-Pei Hsiao[2,5] · Yanuar Haryanto[2,6]

Received: 29 July 2021 / Accepted: 11 January 2022

Abstract

The use of carbon fiber-reinforced polymer (CFRP) rods offers a good solution for external strengthening of flexural reinforced concrete (RC) members. Limited data are available on the behavior of beams externally reinforced with CFRP rods under a loading–unloading protocol, which is of great importance for structural components subjected to vehicle loading. The embedment depth mandated by the majority of standards cannot always be acquired due to concrete cover limitations; the influence of embedment depth under this loading–unloading sequence needs to be investigated. This research studied the effects of rod embedment depth by comparing fully-embedded rods with half-embedded rods under a loading–unloading protocol and comparing the results with monotonic responses. An identical specimen without CFRP reinforcement functioned as the controlling element. The near-surface mounted technique (NSM) was used to integrate the rods with the concrete. The results show that CFRP rods positively affect the load-carrying capacity under a loading–unloading condition. The rods reduce the member's ductility under monotonic loading but have no negative impact under loading–unloading. Whereas the difference in embedment depth configuration slightly affected the enhancement under monotonic loading, the half-embedded rods drastically reduced the capacity improvement under the loading–unloading sequence. An embedment depth deviating from the advised depth, should not be implemented for members subjected to a loading–unloading condition. The CFRP placement method had an impact on the failure behavior of the elements. The half-embedded rod failed by debonding between the rod and the epoxy resin, while the fully-embedded members were characterized by concrete spalling.

Keywords CFRP rods · Flexure · Loading–unloading · Embedment depth

1 Introduction

The improved performance of existing flexural members is required when changes in building codes or alterations in building function demand a higher load-carrying capacity, ductility, or shear proficiency. A range of methods are available, from rigorous demolishing and rebuilding to retrofitting, jacketing, and external strengthening [1–5]. Methods such as the use of haunch elements and jacketing alter the physical appearance of the members and can, therefore, not always be implemented in the field. The application of externally-bonded reinforcement in the tension zone using carbon fiber reinforced polymers (CFRPs) provides a solution to the load-carrying capacity demand while having little to zero impact on the physical exterior of the member.

CFRP rods are durable and attachment to concrete requires much less labor than CFRP sheets and plates. Also, a reduction in the use of a chemical bonding agent (epoxy resin) is significant. The preparation of the concrete surface area

✉ Ay Lie Han
hanaylie@live.undip.ac.id

1 Department of Civil Engineering, Diponegoro University, Semarang, Indonesia

2 Department of Civil Engineering, National Cheng Kung University, Tainan, Taiwan

3 Department of Civil and Disaster Prevention Engineering, College of Engineering and Science, National United University, Miaoli, Taiwan

4 Department of Architecture, College of Engineering, Nihon University, Tokyo, Japan

5 National Center for Research on Earthquake Engineering, Taipei, Taiwan

6 Department of Civil Engineering, Faculty of Engineering, Jenderal Soedirman University, Purwokerto, Indonesia

Published online: 04 February 2022

is much smaller than that of plates and sheets, resulting in a minimization of dust and noise contamination due to the concrete surface grinding process. The CFRP rod behavior is generally linear until failure, with an average tensile strength of 3000 MPa, a modulus of elasticity of 150 GPa, and an ultimate strain of 1.7%. These characteristics are specific to the product used in this research and can vary slightly, according to CFRP type. In combination with a good bonding agent, these rods maintain strain compatibility as a composite with concrete. A number of variables influence the behavior of external reinforcement with rods, i.e. the position of rods relative to the cross section's tensile fibers, the presence of anchorage and end conditions, the axial stiffness of the rods, the reinforcement steel ratio, and position, and their interaction with the rods. Extensive information on these variables, and their impact, can be found in the previous studies [3, 6–11].

An embedment depth of 1.5 times the rod diameter (mandated by the majority of standards) ensures compatibility and guarantees the tensile stress transfer from the concrete to the rods until failure. For older buildings, the concrete cover thickness might be insufficient to warrant this embedment depth, and the groove required to house the rod could dent or even damage the reinforcement. As a result, the rods can only be planted partially into the concrete, reducing the transfer area from the concrete to the rod. The studies on partially and fully-bonded CFRP bars demonstrated that failure was due to concrete cover separation or concrete epoxy failure, depending on the thickness of concrete cover [7, 9]. These findings underline the importance of the relative position of the bars with respect to the concrete surface. The position of rods influences the load-carrying capacity, stiffness, and ductility of the reinforced member. The bond behavior of rods was studied extensively, both in monotonic and cyclic loading [3, 12–16]. However, most of these experiments were conducted with fully-embedded rods or bars. The research by Sharaky et al. [7] and Sharaky et al. [9] provided information on the influence of concrete cover and its confinement, but no data was recorded for loading–unloading schemes.

2 Experimental Work

The research was conducted using beams with a length of 2.5 m, simply supported and subjected to a three-point loading scenario to simulate maximum bending, in combination with maximum shear. Three types of specimen were prepared: a beam without external CFRP reinforcement functions (as a controlling element) (BN), a second beam with two 8 mm CFRP fully-embedded rods (BF), and a third beam where the CFRP rods were embedded for only half of the rod's perimeter (BH). For every category, two specimens were prepared. Since research has shown that the position of the rods with respect to the beam (rods either attached to the bottom or the sides of the member) did not significantly influence the overall behavior [6], bottom placement was chosen in this study. Details of the member are shown in Fig. 1. The details of the rod placement, with respect to the concrete, can be seen in Fig. 2. Figure 2a explains the position of the rod fully embedded into the concrete, while Fig. 2b demonstrates the configuration of a half-embedded rod, with respect to the concrete cover. D is the embedment depth and d' *is* the thickness of the concrete cover.

The CFRP rod embedment depth could significantly influence the capacity enhancement of a member in flexure [7, 9, 12–21]. This paper discusses the responses of the embedment depth and analyzes its effect on the capacity, ductility, member stiffness, and failure mode, based on full-scale, laboratory-tested specimens. Two loading protocols were accessed: monotonic and loading–unloading; the main focus was placed on the loading–unloading protocol. The study also provides an insight into the consequences that arise when the advised embedment depth is not fulfilled while also providing information on the moment deformation, capacity enhancement, and failure mode of these half-embedded rods.

In general, previous studies suggested that the bond strength increased as a function of the rod embedment depth. Direct shear tests conducted on CFRP rods showed that the bond capacity enhancement, as a function of the embedment depth, followed a quadratic, convex pattern [20–22]. The half-embedded rod had the potential of debonding in the interface between the rod and the bonding agent, owing to the limited perimeters of the contact area between the rod and the bonding agent. Half of all the test specimens in the study failed due to debonding. The fully-embedded rods resulted in concrete spalling.

For the experimental investigation, precision instruments were placed to monitor deformations, loads, and strains, for further analysis. The members were all subjected to a monotonic and loading–unloading increment protocol. Five CFRP strain gauges (type FLA 5–11, with a gauge length of 5 mm and a resistance of 120 Ω) were located along the beam's length, while concrete strain gauges (type PL 60–11, with a gauge length of 60 mm and a resistance of 120 Ω) were placed at the extreme tension and compression fibers. To detect the occurrence of buckling, two LVDTs (SD 100-C), with a sensitivity of 50×10^{-6} strain/mm, were used to monitor the vertical deflection of the beam and three LVDTs were used to measure the horizontal deformation of the beam. The load response was measured by a load cell. A three-point bending test was used to generate maximum bending and shear stresses at the midpoint [17, 23–25]. To simulate a negative bending moment in the slab, the beam was turned upside down and the load was induced in a downwards direction. The data were recorded by a data logger (TDS-630) connected to a computer using TDS-7130 software. All of the

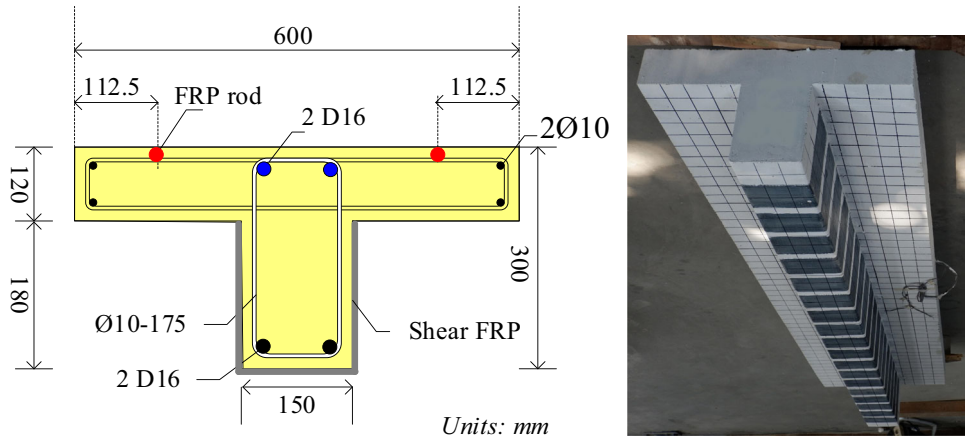

Fig. 1 Specimen details

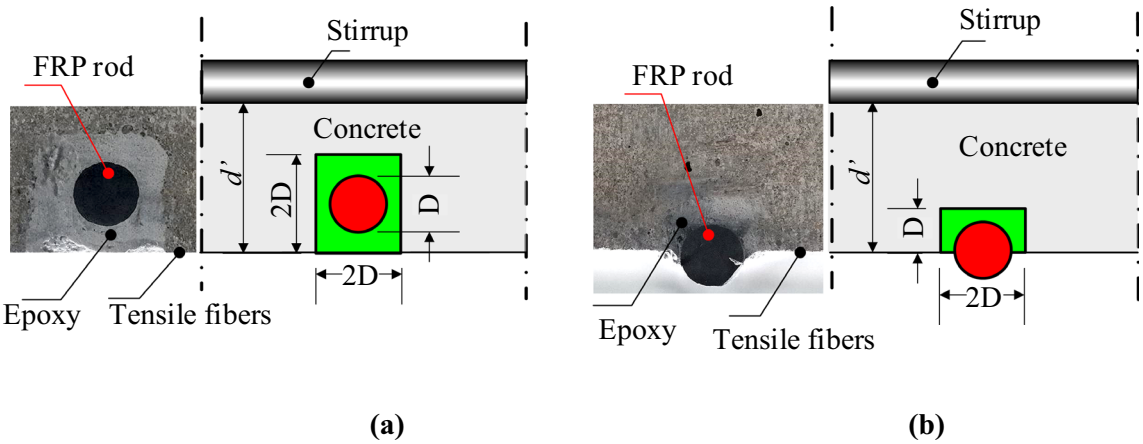

Fig. 2 Description of rod embedment **a** BF and **b** BH

Table 1 Material mechanical properties

Specimen	Dimension (mm)	Compression strength (MPa)	Tensile strength (MPa)	Yield stress (MPa)	Elastic moduli (GPa)
CFRP rod	8	–	3100	–	140
CFRP wrap	0.13	–	3850	–	210
Deformed steel bar D	16	–	727	492	197
Steel bar Ø	10	–	500	350	195
Concrete 28 days	150 × 300	27	–	–	21

measuring equipment used was produced by Tokyo Sokki Kenkyujo, Japan.

The specimens were tested at a concrete age of 28 days. The concrete cylinder strength was measured from six 150 mm × 300 mm cylinders that were prepared during the casting of the beams. The strength f_c' was 27 MPa. The deformed 16 mm reinforcement bars had a yield stress f_y of 492 MPa, in combination with an ultimate strength f_u of 727 MPa. The undeformed 10 mm steel bars had a yield stress f_y of 350 MPa, in combination with an ultimate load f_u of 500 MPa. The mechanical properties of all steel bars were studied using uniaxial coupon tensile tests. The rods were pultruded CFRP rods with a diameter of 8 mm. This type of CFRP has a carbon laminate with a circular cross-section. To ensure failure in bending, the web of the member was reinforced externally using a unidirectional, woven carbon fiber fabric with mid-range strength, designed for installation using the wet application process. The wrap had a thickness of 0.13 mm, minimum tensile modulus of 210 GPa, and mini-

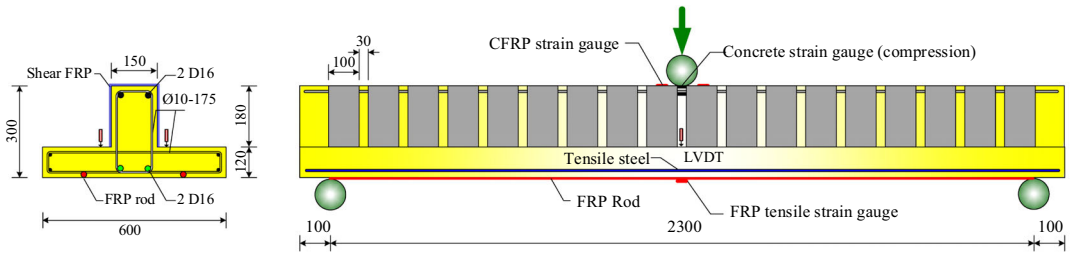

(a)

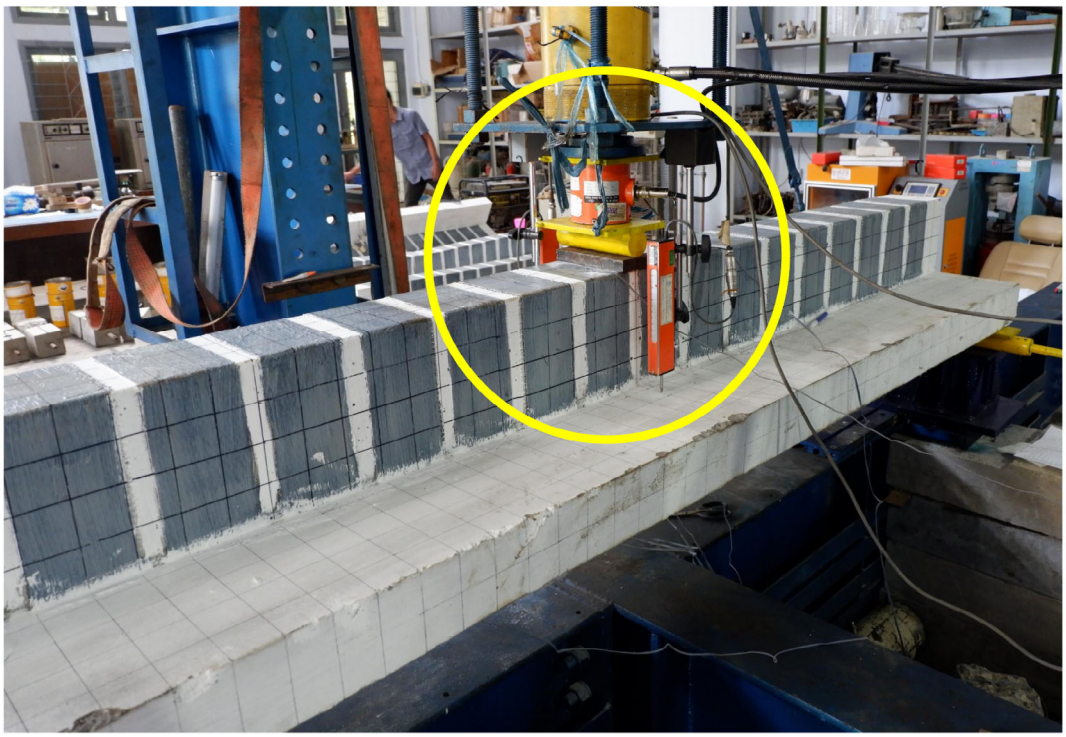

(b)

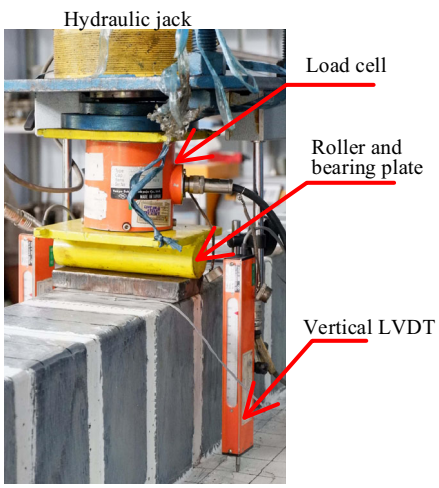

(c)

Fig. 3 Specimen setup **a** Schematic outline **b** laboratory experiment and **c** details of precision instruments

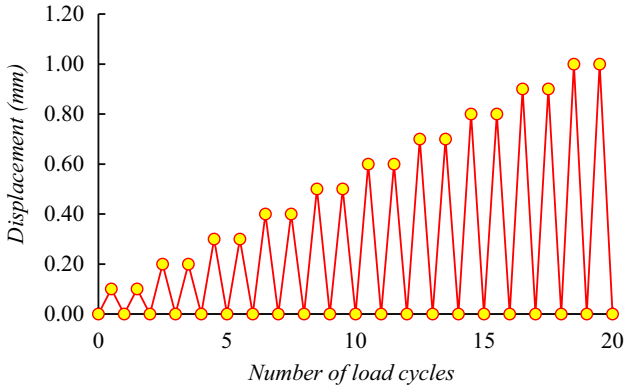

Fig. 4 Loading–unloading increment protocol

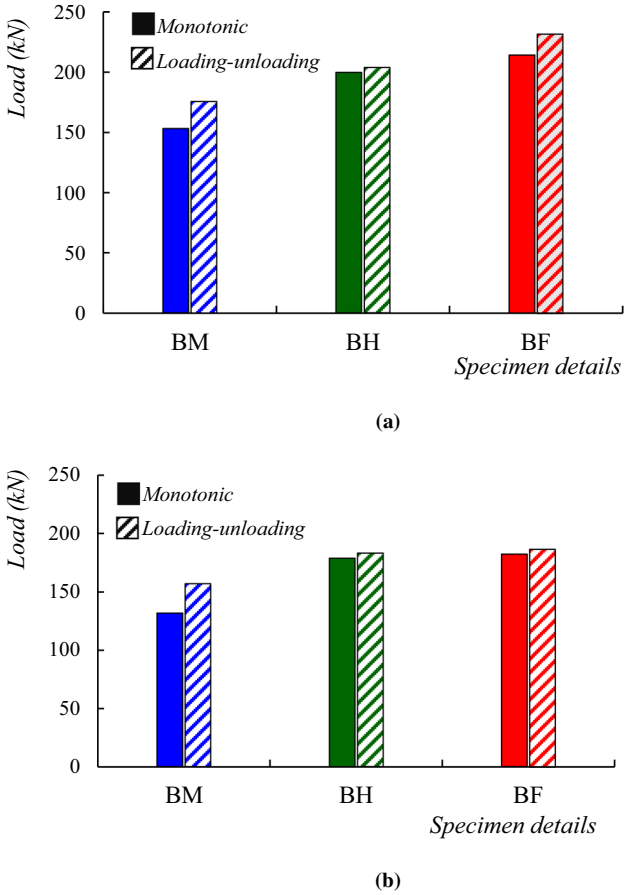

Fig. 5 Monotonic and loading–unloading comparison **a** Ultimate load and **b** yield load

mum tensile strength of 3850 MPa. The data are summarized in Table 1 and the test setup is presented in Fig. 3.

All specimens were tested under monotonic and loading–unloading forces, induced by a hydraulic actuator. The specimens were situated on a rigid platform on the laboratory floor. The supports were two rollers, one with a degree of freedom in the horizontal direction and the other constrained against movement in both the vertical and horizontal directions. The loading setup was deformation controlled, with an increment of 1/10 of the ultimate deformation of BN, generated from the monotonic testing of these control specimens, as shown in Fig. 4. The deformation increment rate at loading and reloading was 4×10^{-4} m/sec.

3 Results and Discussion

The data obtained from the tests were compiled and presented as the load-vertical deformation relationship in monotonic and loading–unloading sequences. Furthermore, the improvement in load carrying capacity, load levels at first yielding, ultimate deformation, and the initial stiffness of the members and its evolution pattern were evaluated. The failure mode of the three beam types was investigated and a comparison between the monotonic and loading–unloading protocols was conducted.

3.1 Ultimate and Yield Load

The ultimate load was obtained from the data recorded by the load cell. In general, the fully-embedded specimen BF exhibits the largest load-carrying capacity, followed by the half-embedded specimen BH. Table 2 shows the ultimate load and increase ratios with respect to each controlling element. The actual ultimate and yield load comparisons are shown graphically in Fig. 5a for monotonic loading, and Fig. 5b for loading–unloading. The determination of the yield load level was based on the strain gauge readings attached to the tensile reinforcing steel. For all categories, yielding occurred at 85% to 90% of the ultimate load.

Under monotonic loading, the increase in ultimate load compared to the control element (BN) was 30% for the half-embedded section (BH) and 40% for the full-embedded element (BF). The deviation in embedment depth had little effect on the load-carrying capacity of the member and a deviation of 25% resulted. The loading–unloading sequence created microcracks in the concrete interface and, because of the relatively small contact area of the rod, impacted on the improvement of load-carrying capacity. The load at which steel yielding occur for both the loading protocols were closely approaching one and another. On average, the monotonic testing resulted in slightly lower loading compared with the loading–unloading, for all three types of test elements. This phenomenon was the result of earlier strain-hardening in the tensile steel for the monotonic loading, compared to the loading–unloading process. In contrast, for the loading–unloading protocol, the improvement was only 16% for BH, while the BF reached an enhancement of 32%. For the loading–unloading scheme, the magnitude of the transfer area between the concrete and the rod strongly influenced the

Table 2 Ultimate and yield load

Specimen	Monotonic				Loading–unloading			
	Ultimate		Steel yield		Ultimate		Steel yield	
	Actual load (kN)	$\frac{P_{ult}}{P_{BN}}$	Actual load (kN)	$\frac{P_{yield}}{P_{ult}}$	Actual load (kN)	$\frac{P_{ult}}{P_{BN}}$	Actual load (kN)	$\frac{P_{yield}}{P_{ult}}$
BN	153.14	1.00	131.75	0.86	175.57	1.00	157.04	0.89
BH	199.80	1.30	178.96	0.90	203.67	1.16	183.31	0.90
BF	214.13	1.40	182.31	0.85	231.40	1.32	186.43	0.81

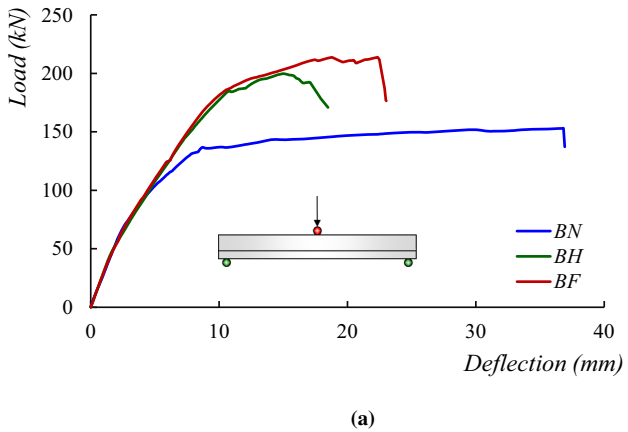

(a)

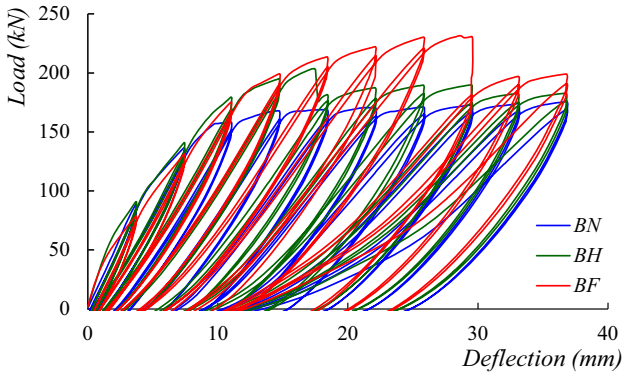

(b)

Fig. 6 Load–deformation responses **a** Monotonic and **b** Loading–unloading

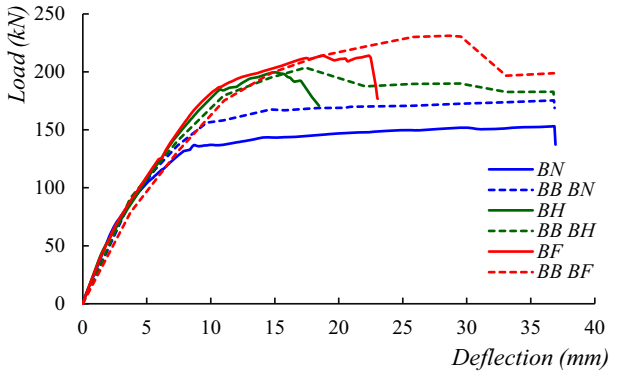

Fig. 7 Load deformation (monotonic) versus backbone (loading–unloading)

effectiveness of the rod in accommodating the tensile strains from the concrete.

3.2 Load–Deformation Response

The load–displacement responses of both loading scenarios are shown in Fig. 6a, for monotonic loading, and in Fig. 6b, for loading–unloading.

Monotonic loading resulted in a clear yielding pattern for the control element (BN) and the mechanism of the rod-reinforced members behaved differently due to the stress redistribution in the tensile region of the beam (Fig. 6a). The presence of rods altered the deformation rate and resulted in a delay in the steel bar yielding process. After yielding, the tensile stresses originally carried by the reinforcing steel were redistributed to the rods. While the initial stiffness of the three members was not influenced significantly by the presence of rods, the curves for BH and BF demonstrated a higher stiffness approaching yielding, with no distinguishing yield plateau after yielding. Both CFRP-reinforced specimens also exhibited a reduction in ultimate deformation and specimen BF presented a better ductility than BH. Figure 6b represents the loading–unloading of the elements. The load-deformation of the BHs and BFs closely approached the response of BN, except for a higher load-carrying capacity. The ultimate displacement was recorded as 36.8 mm, 17.4 mm, and 28.7 mm for BN, BH, and BF, respectively.

The backbone response of the loading–unloading protocol versus the monotonic scheme is presented in Fig. 7.

The dotted lines represent the backbone response of the loading–unloading versus the monotonic data for each specimen, and the notation BB represents the backbone curves. The initial stiffness remained unchanged and the member stiffness developed in a similar pattern for both the monotonic and loading–unloading protocols. For the CFRP rod-reinforced members, the loading–unloading protocol resulted in a more gradual yielding of the tensile reinforcement, due to the moderate increase in deflection. The ultimate

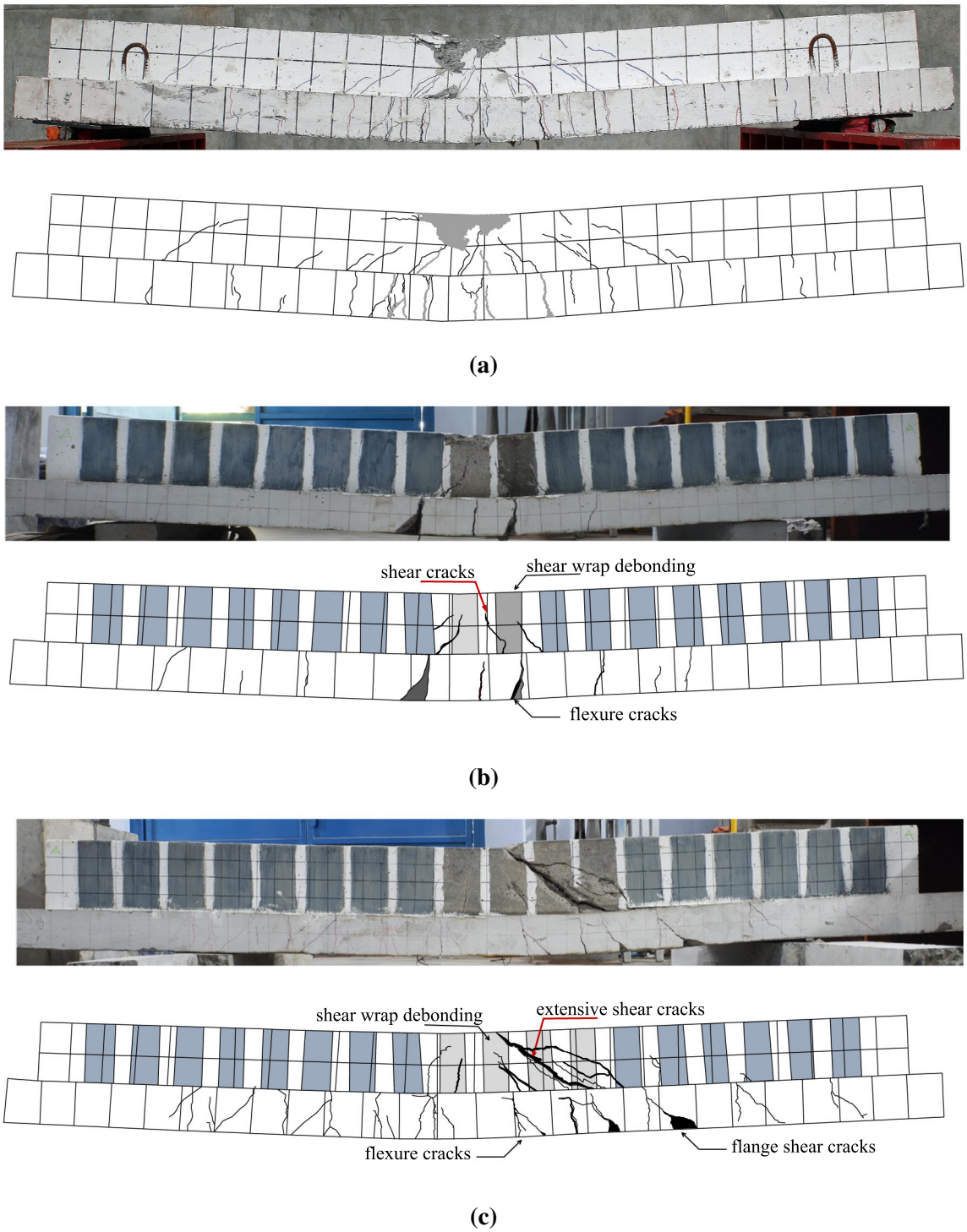

Fig. 8 Failure mode **a** control element **b** flexure cracks (BH) and **c** flexure–shear cracks (BF)

deformation of all members approached the ultimate deformation of the control element.

3.3 Failure Mode

Based on the observations, all elements failed as under-reinforced members, characterized by tensile steel yielding. Reaching one-third of the ultimate load, the first cracks were

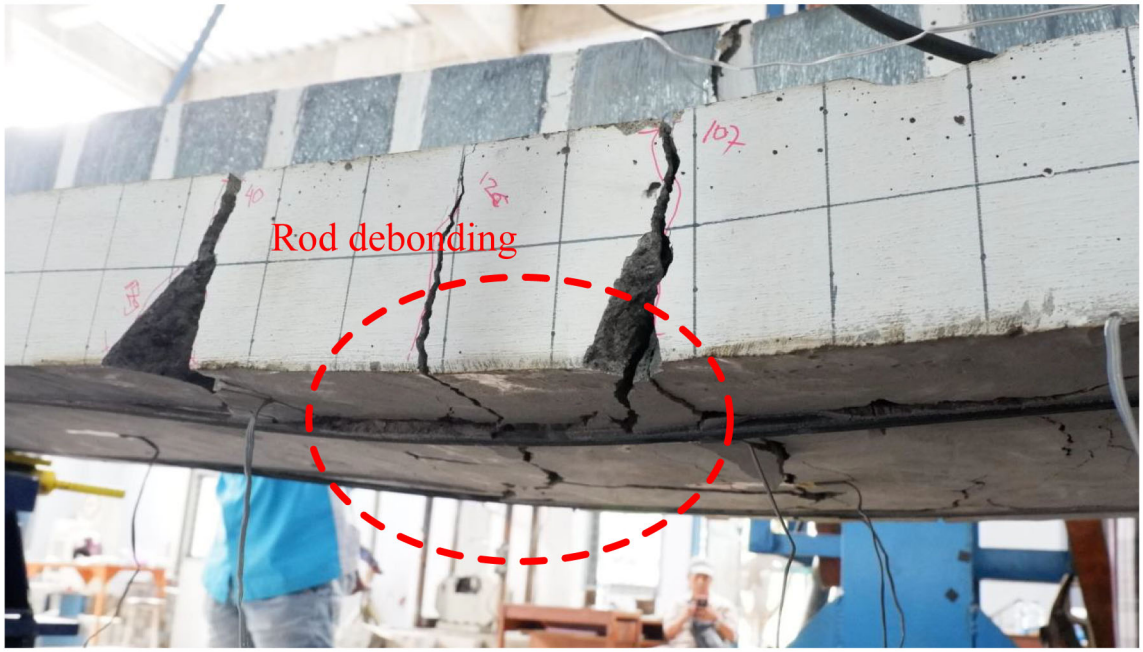

(a)

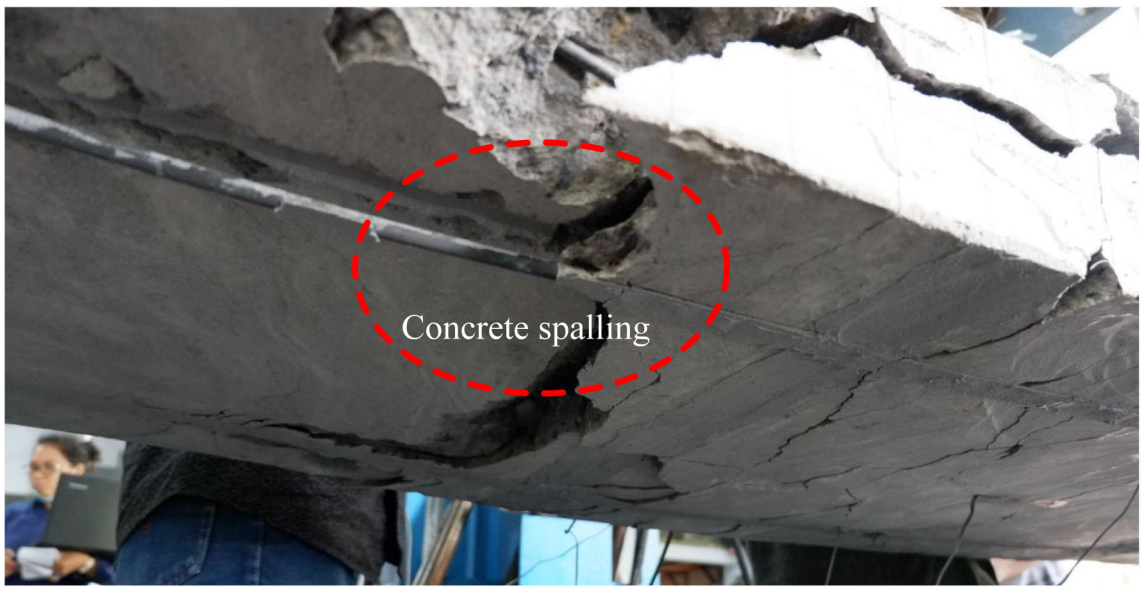

(b)

Fig. 9 Rod behavior at failure **a** debonding (BH) and **b** concrete spalling (BF)

observed at the maximum tensile area of all specimens. For the BN specimen, this was followed by yielding of the reinforced tensile steel at load levels closely approaching the members' ultimate load-carrying capacity. The steel yields a reduction in the concrete compression area due to extensive crack widening and crack propagation toward the neutral axis. During further stages, the tensile steel continued to yield, which can be seen as the post-peak in Fig. 6a. The strain in the concrete increased and approached the ultimate compression strain; the concrete failed due to the crushing of the mortar matrix.

Studying the behavior of specimens (BH) with half-embedded CFRP rods and BF with fully embedded CFRP rods, it was shown that the level at which the first cracks

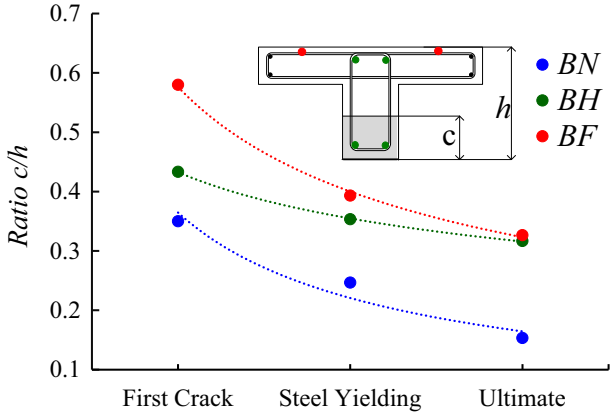

Fig. 10 Neutral axes shifting

occurred was almost identical to that of BN (Fig. 8a). Concrete cracking was measured at 30% and 40% of the ultimate load for BHs and BFs, respectively. Specimen BF had a better crack performance since the fully-embedded rod contributed to the overall stiffness of the section. It was interesting to observe that the external reinforcement had an insubstantial influence on both the ultimate and tensile steel yielding (see Table 2). Ultimately, the bond between the CFRP bars and the epoxy for the BH member failed by shearing: the tensile steel yielded and failure occurred soon after. A mild yield plateau was detected. The specimen demonstrated severe flexure cracks at the midpoint (Fig. 8b). BF was characterized by flexure-shear failure, in combination with large diagonal cracks that propagated from the tensile fibers of the concrete at and around the midpoint, up to the compression zone. These findings were strengthened by the research of Sallam et al. [26], who investigated the peeling of externally plated beams. The bond between the FRP rods could withstand the strain differentiations but the concrete at the interface failed in shear (Fig. 8c). The external shear reinforcement lost its bond, enabling the shear cracks to expand beyond the neutral axis. The compatibility between the rods and concrete was preserved until failure due to the remaining bond at the far ends of the member functioning as a pre-tensioning element. The difference between the failure modes of the BHs and BFs is shown in Fig. 9. All of the failure modes of the rod-reinforced members were sudden.

3.4 Neutral Axis Deviation

Direct shear-bond tests on identical rods and concrete [20, 21] suggested that the influence of the embedment depth increase followed a quadratic convex path. The failure stresses that occurred in the fully-embedded rods were three times higher than those of the half-embedded rods. The fully-embedded rods failed in the concrete due to spalling, while the half-embedded rods failed in the interface between the epoxy agent and the concrete. These findings justify the results of the test on the beam elements. Neither of the externally-reinforced beams, BH and BF, exhibited a clear yield plateau as a consequence of the intervention of the CFRP, which behaved linearly up until failure. The initial stiffness of all members was identical. After the first cracking and propagation, the CFRP-reinforced members had a gradual reduction in member stiffness.

The use of external reinforcement influences the shifting of the neutral axis (Fig. 10): the larger the embedment depth of the rods, the more significant the shifting of the axis towards the tensile zone. This, in turn, had a significant influence on the failure mode of the specimens. The rod that was placed with a full embedment depth failed in flexure-shear failure after the yielding of the steel bars and rupture of concrete in the vicinity of the rods.

The theoretical balance steel ratio (ρ_b) for the BN element was calculated and found to be 0.0081, whereas the existing conventional steel reinforcement ρ_S was 0.0057. For the CFRP-reinforced specimen BF, the balanced CFRP reinforcement ratio ρ_{bFRP} was found to be 0.0009. The two 8 mm rods, however, resulted in a ratio of 0.0010, which was above the balance ratio. Technically, the element was bound to fail as an over-reinforced member. The experimental test data contradicted this statement because both the BF and the BH beams exhibited yielding in conventional reinforced steel, characterizing under-reinforced behavior. From this observation, it is concluded that the connection of the rod to the concrete cannot be considered to have been fully bonded, and this semirigid state probably originated from the behavior of the epoxy resin surrounding the rod.

The fully-embedded element BF did not exhibit debonding. The bond provided additional confinement to the member in the longitudinal direction. Studies of the end conditions and development length of CRFP rods [6, 8, 10] have shown that the failure behavior of the member was dependent upon the end conditions, explaining the behavior of the BF member. Furthermore, the CFRP shear reinforcement created a confining effect within the concrete compression zone, enhancing its cylinder compression strength by up to 20%. These confinements shifted the failure mode from flexure to flexure–shear and large diagonal cracks extended up to the compression area of the member. The decrease in the moment of inertia resulted in large deflections that led to yielding in the steel bars. Finally, the concrete interface surrounding the rod failed in shear.

4 Conclusion

This study of the loading–unloading of externally-reinforced flexural members using CFRP rods concluded that the effect of rod-embedment depth variation was less under mono-

tonic loading, but significantly influenced the load-carrying capacity under loading–unloading protocols. For monotonic loading, the fully-embedded rod yielded in a 40% capacity increase and a 32% enhancement for the loading–unloading scheme. It can be seen that the fully-embedded rod provided a good performance for the loading–unloading protocol. On the contrary, under monotonic loading, the half-embedded rod increased the load-carrying capacity by 30%, but only by 16% for the loading–unloading conditions. These results demonstrate that the loading–unloading scheme is sensitive to the relative position of the rod. Under monotonic loading, the capacity decrease was 25%, whereas for the loading–unloading it reached a 50% decline. The placement of the rod is ineffective for members subjected to a loading–unloading condition and an embedment depth less than the mandated depth should be avoided for these structural elements.

The presence of rods altered the ultimate displacement of the specimens under monotonic loading in a negative manner and no clear yielding pattern was observed after yielding of the steel reinforcement. For the loading–unloading (based on the backbone pattern), the rods had little influence on the ultimate displacement.

The embedment depth modified the failure mode. Fully-embedded rods failed due to concrete spalling in the vicinity of the maximum tensile strains. The bonds between the rod and epoxy and the epoxy and the concrete withstood the strain disparities until failure. After spalling in the maximum moment region, the bond and concrete at the far ends remained undisturbed and provided confinement in the longitudinal direction of the member, resulting in a moderate deformation rate and prolonged failure of the member. The half-embedded rod failed due to debonding between the rod and the epoxy resin because of the limited contact area. No shear cracks were detected and the debonding propagated to the far ends of the rod.

Fully-embedded CFRP rods contributed significantly to the increase in load-carrying capacity for monotonic, as well as loading–unloading, scenarios. The deformation behavior under loading–unloading was close approaching the unreinforced members, providing good ductility. However, the placement of partially embedded rods is not recommended for structures subjected to loading–unloading schemes, such as vehicles and machinery. Half-embedded rods may be used for housing structures, on condition that the application methods, preparation of the groove, concrete surface cleaning and application, and compaction of the epoxy bonding agent are precisely monitored.

Author Contributions HAL is the main researcher and author of this work. She designed the research methodology and was responsible for the overall experimental testing, data collection, and data processing. HTH performed the data compiling and was responsible for all data interpretations and visual readings during and after the experiments. BSG concentrated on the data processing, resulting in the final conclusion, and presented all graphical figures presented in this work. FPH constructed all calculations and visualizations, resulting in the relationship graphs and tables, and supported the data analysis process, especially for the loading–unloading protocol. YH was the researcher responsible for specimen setup, operating the reading equipment, and controlling all precision instruments.

Declarations

Conflicts of interest The authors have no conflicts of interest to declare.

Data availability The data and material presented in this paper are available for use by researchers in this field and might be used with proper citations.

References

1. Han, A.L.; Utomo, J.; Hu, H.-T.; Lestari, L.T.: Seismic retrofitting of irregular pre-80s low-rise conventional RC building structures. Civ. Eng. Dimens. **23**, 9–19 (2021). https://doi.org/10.9744/ced.23.1.9-19
2. Purwanto, H.A.L.; Ekaputri, J.J.; Nuroji, P.B.H.: Self-compacting-geopolymer-concrete SCGC retrofitted haunch. Int. J. Eng. Appl. (2021). https://doi.org/10.15866/irea.v9i4.20652
3. Sharaky, I.A.; Selmy, S.A.I.; El-Attar, M.M.; Sallam, H.E.M.: The influence of interaction between NSM and internal reinforcements on the structural behavior of upgrading RC beams. Compos. Struct. **234**, 111751 (2020). https://doi.org/10.1016/j.compstruct.2019.111751
4. Amran, Y.H.M.; Alyousef, R.; Rashid, R.S.M.; Alabduljabbar, H.; Hung, C.-C.: Properties and applications of FRP in strengthening RC structures: a review. Structures **16**, 208–238 (2018). https://doi.org/10.1016/j.istruc.2018.09.008
5. Peiris, A.; Harik, I.: Design and construction of CFRP rod panel retrofit for impacted RC bridge girders. J. Compos. Sci. **2**, 1–19 (2018). https://doi.org/10.3390/jcs2030040
6. Sharaky, I.A.; Reda, R.M.; Ghanem, M.; Seleem, M.H.; Sallam, E.M.: Experimental and numerical study of RC Beams strengthened with bottom and side NSM GFRP bars having different end conditions. Constr. Build. Mater. **149**, 882–903 (2017). https://doi.org/10.1016/j.conbuildmat.2017.05.192
7. Sharaky, I.A.; Baena, M.; Barris, C.; Sallam, H.E.M.; Torres, L.: Effect of axial stiffness of NSM FRP reinforcement and concrete cover confinement on flexural behaviour of strengthened RC Beams: experimental and numerical Study. Eng. Struct. **178**, 987–1001 (2018). https://doi.org/10.1016/j.engstruct.2018.07.062
8. Reda, R.M.; Sharaky, I.A.; Ghanem, M.; Seleem, M.H.; Sallam, H.E.M.: Flexural behavior of RC beams strengthened by NSM GFRP bars having different end conditions. Compos. Struct. **147**, 131–142 (2016). https://doi.org/10.1016/j.compstruct.2016.03.018
9. Sharaky, I.A.; Torres, L.; Sallam, H.E.M.: Experimental and analytical investigation into the flexural performance of RC beams with partially and fully bonded NSM FRP bars/strips. Compos. Struct. **122**, 113–126 (2015). https://doi.org/10.1016/j.compstruct.2014.11.057
10. El-Emam, H.; El-Sisi, A.; Bneni, M.; Seleem, S.E.A.; Sallam, H.E.M.: Effects of tensile reinforcing steel ratio and near-surface-mounted bar development length on the structural behavior of strengthened RC beams. Lat. Am. J. of Solids Struct. (2020). https://doi.org/10.1590/1679-78255836

11. Reda, R.M.; Omar, Z.; Sallam, H.E.M.; Seleem, S.E.A.: Effect of different parameters controlling the flexural behavior of RC beams strengthened with NSM using nonlinear finite element analysis. Frat. Integrita Strutt. **14**, 106–123 (2020). https://doi.org/10.3221/IGF-ESIS.53.09
12. Gómez, J.; Torres, L.; Barris, C.: Characterization and simulation of the bond response of NSM FRP reinforcement in Concrete. Materials **13**, 1770-1-1770–21 (2020). https://doi.org/10.3390/ma13071770
13. Caro, M.; Jemaa, Y.; Dirar, S.; Quinn, A.: Bond performance of deep embedment FRP bars epoxy-bonded into concrete. Eng. Struct. **147**, 448–457 (2017). https://doi.org/10.1016/j.engstruct.2017.05.069
14. Diab, H.M.A.; Abdelaleem, T.; Rashwan, M.M.M.: Moment redistribution and flexural performance of RC continuous T-beams strengthened with NSM FRP or steel bars. Structures **28**, 1516–1538 (2020). https://doi.org/10.1016/j.istruc.2020.09.003
15. Abdallah, M.; Al Mahmoud, F.; Khelil, A.; Mercier, J.; Almassri, B.: Assessment of the flexural behavior of continuous RC beams strengthened with NSM-FRP bars, experimental and analytical study. Compos. Struct. **242**, 112127-1-112127–23 (2020). https://doi.org/10.1016/j.compstruct.2020.112127
16. Abdallah, M.; Al Mahmoud, F.; Boissière, R.; Khelil, A.; Mercier, J.: Experimental study on strengthening of RC beams with side near surface mounted technique-CFRP bars. Compos. Struct. **234**, 111716 (2020). https://doi.org/10.1016/j.compstruct.2019.111716
17. Haryanto, Y.; Hu, H.-T.; Han, A.L.; Hsiao, F.-P.; Teng, C.-J.; Hidayat, B.A.; Wariyatno, N.G.: Negative moment region flexural strengthening system of RC T-beams with half-embedded NSM FRP rods: a parametric analytical approach. J. Chin. Inst. Eng. **44**, 553–561 (2021). https://doi.org/10.1080/02533839.2021.1936646
18. Haryanto, Y.; Hu, H.-T.; Han, A.L.; Hsiao, F.-P.; Teng, C.-J.; Hidayat, B.A.; Nugroho, L.: Nonlinear 3D model of double shear lap tests for the bond of near-surface mounted FRP rods in concrete considering different embedment depth. Period. Polytech. Civ. Eng. **63**, 878–889 (2021). https://doi.org/10.3311/PPci.17309(gantiCAC)
19. Sapulete, C.A.: Experimental Study the Effect of FRP Rods and Wrap as a Flexural Strengthening on the RC Beams. Master Thesis, Diponegoro University, Indonesia (2018)
20. Han, A.L.; Gan, B.S.; Budipriyanto, A.: Shear-bond behavior of fiber reinforced polymer (FRP) rods and sheets. MATEC Web Conf. **195**, 02001-1-02001–7 (2018). https://doi.org/10.1051/matecconf/201819502001
21. Budipriyanto, A.; Han, A.L.; Hu, H.-T.: Bond-shear behavior of FRP rods as a function of attachment configuration. J. Adv. Civ. Environ. Eng. **1**, 9–17 (2018). https://doi.org/10.30659/jacee.1.1.9-17
22. Wang, X.; Cheng, L.: Bond characteristics and modeling of near-surface mounted CFRP in concrete. Compos. Struct. **225**, 113011-1-113011–13 (2021). https://doi.org/10.1016/j.compstruct.2020.113011
23. Tudjono, S.; Han, A.L.; Gan, B.S.: An integrated system for enhancing flexural members' capacity via combinations of the fiber reinforced plastic use, retrofitting, and surface treatment techniques. Int. J. Technol. **9**, 5–15 (2018). https://doi.org/10.14716/ijtech.v9i1.298
24. Haryanto, Y.; Hu, H.-T.; Han, A.L.; Hsiao, F.-P.; Teng, C.J.; Hidayat, B.A.; Nugroho, L.: Numerical investigation on RC T-beams strengthened in the negative moment region using NSM FRP rods at various depth of embedment. Comput. Concr. (2021). https://doi.org/10.12989/cac.2021.28.4.000
25. Tudjono, S.; Han, A.L.; Gan, B.S.: Revitalization of cracked flexural members using retrofitting and synthetic wrapping. Procedia Eng. **171**, 1123–1128 (2017). https://doi.org/10.1016/j.proeng.2017.01.472
26. Sallam, H.E.M.; Saba, A.M.; Shahin, H.H.; Abdel-Raouf, H.: Prevention of peeling failure in plated beams. J. Adv. Concr. Technol. **2**, 419–429 (2004). https://doi.org/10.3151/jact.2.419